

Chapter 9. Upwelling

Pablo Clemente-Colón

Office of Research and Applications, NOAA/NESDIS, Camp Springs, MD, USA

9.1 Introduction

Ocean upwelling is the ascending motion of water from subsurface layers resulting from horizontal divergence at the surface layer and convergence below [Smith, 1968]. A more restrictive definition can be adopted by which upwelling is described as the “upward penetration of a mass of water into a surface mixed layer” and coastal upwelling, in particular, can be described as “the rise of the thermocline toward the coast” [Yoshida and Mao, 1957]. Detection and monitoring of upwelling activity from space over the world’s oceans is of importance as these regions are characterized by very high primary productivity and sustain roughly about half of the world’s fisheries catch, while accounting for only about 1 percent of the ocean surface area. Upwelling dynamics are also considered a significant mechanism in the marine biogeochemical cycling of carbon and nitrogen and have important implications to local surface property fluxes and weather.

Upwelling activity commonly happens in coastal regions in response to wind forcing parallel to the coastline that produces a net surface water mass transport to the right of the wind direction in the Northern Hemisphere, to the left in the Southern Hemisphere, due to the Coriolis effect caused by Earth’s rotation. Areas of intense upwelling activity are typically observed extending offshore from continental shelf regions that experience strong favorable winds throughout extended periods of time. These include the United States (U.S.) west coast and northwest coast of Mexico, the coast of Ecuador and Peru, the northwest and southwest coasts of Africa, and the east coast of Somalia and the Arabian Peninsula. Additional areas of less intense or shorter duration coastal upwelling activity are also found in many places around the world. Wind forcing over the equatorial ocean regions can produce ocean surface divergence and consequently upwelling, where the Equator itself serves as a boundary analogous to the coastline in coastal upwelling. Open ocean upwelling may also be induced by atmospheric pressure changes such as those imposed by low-pressure storm systems. In addition to atmospheric forcing, ocean currents can produce upwelling through current interaction with bathymetry that induces vertical mixing, sometimes referred to as tidal pumping, and through geostrophic adjustments of the mean circulation, known as dynamic uplift. Current-driven upwelling is in general independent of wind forcing although a combination of both atmospheric and current effects may enhance the upwelling conditions observed in some regions.

Generally, upwelling is a seasonal or intermittent process that leads to significant changes in water mass distribution in the upper layers. As the thermocline rises and in many cases reaches the surface, the vertical temperature gradient is decreased. Changes in the subsurface density structure produce significant changes in the properties of the surface waters. These properties can be detected and monitored through a variety of in-situ or satellite instruments. Satellite observations of upwelling indicators have the advantage of providing a synoptic view of a region compared to the limited spatial coverage afforded by in-situ sensors.

The focus of this chapter is on the capabilities and limitations of spaceborne synthetic aperture radar (SAR) as a tool to detect ocean surface signatures associated with upwelling

activity. After a brief discussion of upwelling surface effects and their detection from space, a series of SAR upwelling signatures from the U.S. west coast, a major upwelling region, and the U.S. east coast, a minor upwelling region, are then examined. These data are interpreted vis-à-vis thermal infrared (IR) and visible observations currently used to routinely detect and monitor upwelling activity.

9.2 Upwelling and its Effect on Surface Water Properties

Ekman [1905] deduced the fundamental dynamics of wind-forced upwelling from looking at the deflection in the drift of icebergs. A balance between wind frictional forcing at the sea surface and the Coriolis forcing due to Earth's rotation explained the observed current deflection. The Coriolis force deflects the motion of currents to the right in the Northern Hemisphere and to the left in the Southern Hemisphere within the time-scale of an inertial period. Surface wind forcing imposes a shearing stress in the water. The resulting total water mass transport, also referred to as the Ekman transport, has a mean transport direction to right (left) of the wind stress direction in the Northern (Southern) Hemisphere. If there is a barrier such as the coast to the left of the wind direction (to the right in the case of the Southern Hemisphere), the divergent horizontal Ekman transport at the surface can produce a significant compensating upward flow, hence the term upwelling (Figure 9.1).

The presence of stratification (i.e., a mixed layer and thermocline) is required under the definition of upwelling used here. For coastal upwelling and assuming two-layer stratification, the average upwelling speed (vertical movement) at the base of the upper layer is estimated to be of the order of 10^{-3} cm s⁻¹ [*Smith*, 1968]. This upward movement typically brings low temperature, high nutrient, low oxygen, and in most cases lower salinity waters to the upper layer. The process creates anomalies in the surface distribution of these physical and chemical properties. These surface anomalies serve as indicators of upwelling dynamics. Since upwelling brings nutrients into the euphotic zone, it also significantly enhances the primary productivity of coastal waters, which further contributes to changes in the bio-optical properties of the surface water mass such as an increase in the chlorophyll-a (Chl-a) content. The presence of upwelling can be detected through in-situ, airborne or spaceborne sea surface observations of the distribution of these properties. The strength of upwelling may be further assessed by comparing measurements of properties inside with measurements outside the effective width of the upwelling region.

9.3 Upwelling Observations from Space

The ability to spatially map and monitor upwelling activity is important because of both its effect on coastal productivity and its contribution to the marine biogeochemical cycling of carbon and nitrogen, the cross shelf transport of properties and pollutants, and the exchange of properties across the air-sea interface. Under cloud-free conditions, routine observations of upwelling are currently being done from space through passive observations made in the thermal-IR and in the visible part of the electromagnetic spectrum. Observations of sea surface temperature (SST) from thermal-IR sensors such as the NOAA Advanced Very High Resolution Radiometer (AVHRR) are the most commonly used to map areas of active upwelling. Ocean color products such as Chl-a or fluorescence from satellite visible (ocean color) sensors like the Sea-viewing Wide Field-of-view Sensor (SeaWiFS), the Moderate Resolution Imaging Spectroradiometer (MODIS), or the Medium Resolution Imaging Spectrometer (MERIS) are also useful in detecting and mapping upwelling activity through its effects on biological activity.

Upwelling

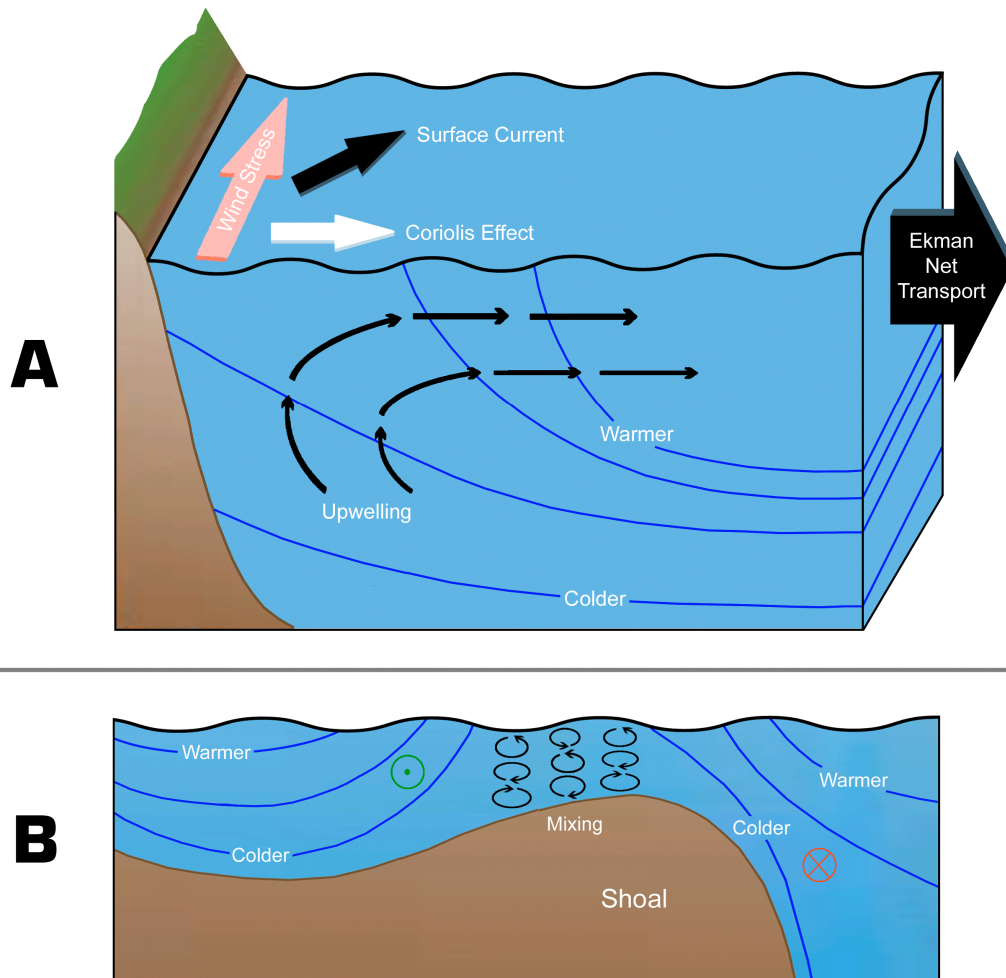


Figure 9.1. a) Schematic of wind-forced coastal upwelling in the Northern Hemisphere indicating the direction of the wind stress relative to the coastline, the surface drift direction (45° to the right of the wind direction), the offshore direction of the Coriolis effect and net Ekman transport, the raising of isotherms toward the coast, and the inshore upwelling circulation. b) Schematic of current-induced upwelling over shallow bathymetry indicating the raising of isotherms over a shoal as flow induces water mixing. An offshore current flowing into the page and an over the shelf current flowing out of the page are also depicted in the figure.

In the case of SAR, the key mechanisms for imaging upwelling patterns are 1) the reduction of sea surface roughness due to lower sea surface temperatures that decrease the wind stress and 2) the presence of upwelling-associated biogenic slicks and the ensuing damping of capillary and gravity (Bragg) waves. In the first mechanism, colder waters resulting from upwelling can impose significant changes in the stability of the marine boundary layer as well as in the surface water density relative to the surrounding waters. Lower wind stress produced by increased stability (i.e., colder sea level temperatures) and by possible increased damping of capillary waves over colder and denser waters contribute to produce lower sea surface roughness, thus creating areas of lower backscatter in SAR imagery. In the second mechanism, biogenic slicks that dampen the sea surface roughness are caused by biological activity associated with the higher concentration of nutrients in the upwelled waters and the increased availability of sunlight at the surface layer. Thus, the imaging of upwelling patterns by SAR may result from both thermal and biological effects. The interpretation of SAR imagery over upwelling regions

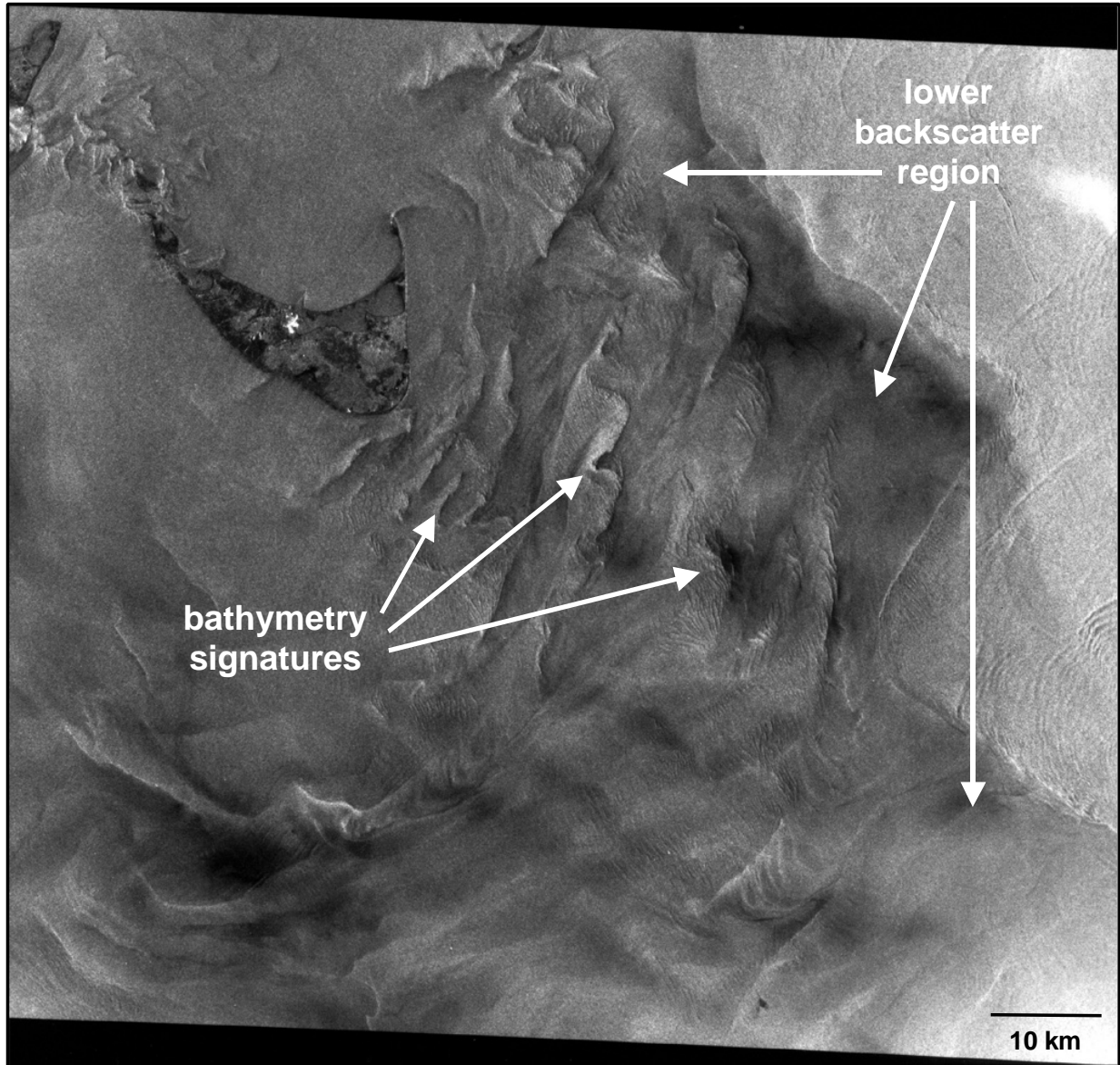


Figure 9.2. SEASAT (L-band, HH) SAR image of the Nantucket Shoals, south of Cape Cod, Massachusetts, acquired on 27 August 1234 UTC. Nantucket Island is shown in the upper-left quadrant of the image. The decrease in backscatter over the region was suggested by *Apel* [1987] to be the result of SAR sensitivity to upwelling conditions. Bathymetric patterns and oceanic internal waves are also evident in this image. [Image courtesy of NASA/JPL]

is unfortunately complicated by other atmospheric and oceanic factors such as low wind speeds, rain, or the presence of mineral surfactants that also cause the occurrence of low radar backscatter features [*Clemente-Colón and Yan, 2000*].

Since the advent of the first spaceborne SAR aboard SEASAT, certain circulation patterns imaged by this active microwave imaging sensor have been linked to upwelling activity. These observations are of interest since a SAR is not limited to operating under cloud free conditions, like thermal and visible sensors. *Fu and Holt* [1982] showed circulation patterns captured by SEASAT indicating the offshore intrusion of shelf water and associated coastal eddies that result from the seasonal upwelling dynamics off Point Arena, California. However,

Upwelling

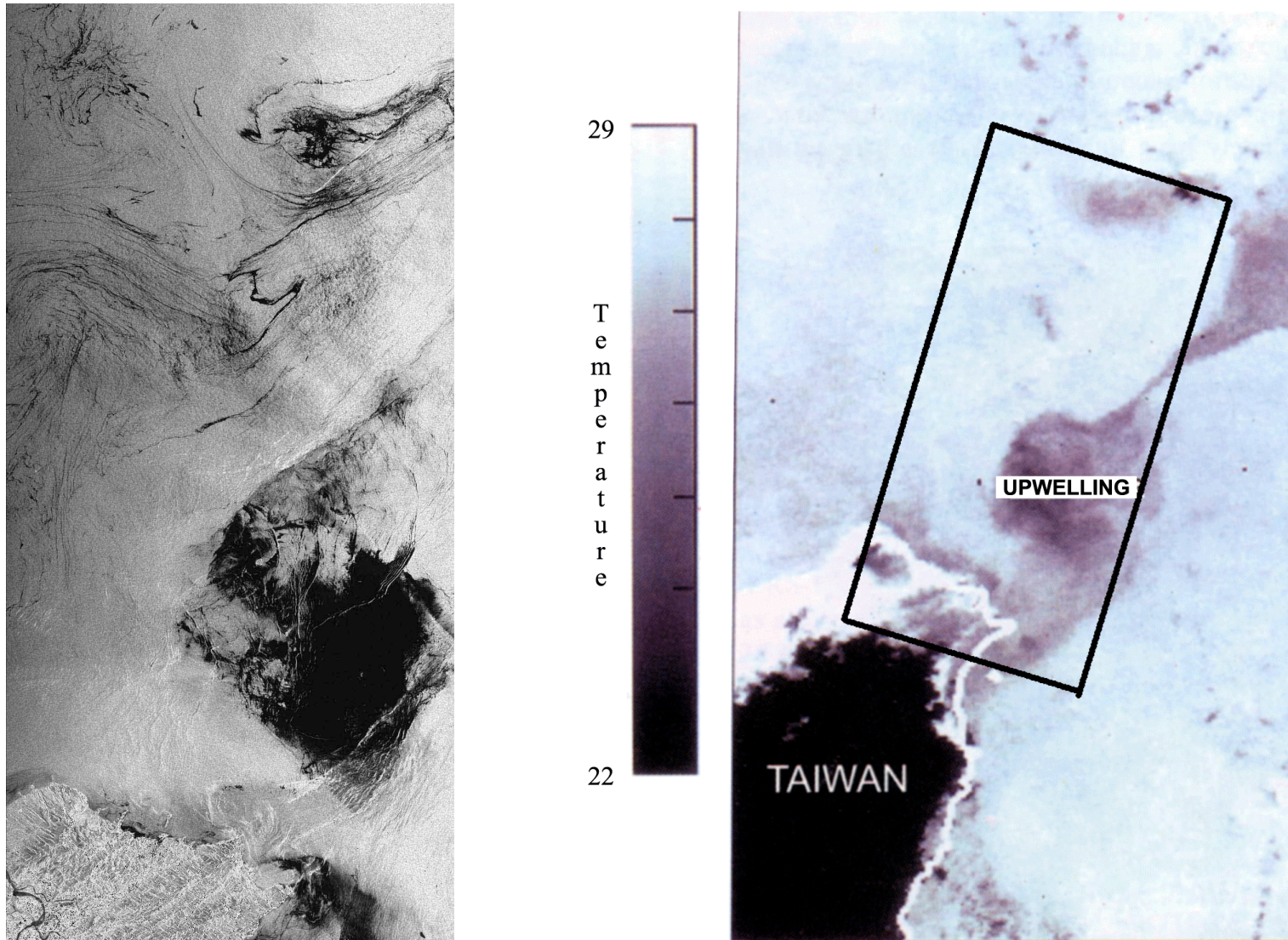


Figure 9.3. ERS-1 (C-Band, VV) SAR image (left) off the Northern coast of Taiwan acquired on 23 July 1994 at 0226 UTC and NOAA-11 AVHRR SST image in °C (right) acquired 22 July 1994 at 0803 UTC. The predominant low backscatter feature is interpreted as an indication of upwelling induced by the Kuroshio Current interaction with bathymetry [After *Hsu et al.* 1995, 2000]. The ERS imaged area is 200 km x 100 km with its coverage outlined on the SST image. ERS image ©ESA 1994, courtesy of The Tropical and Subtropical Ocean Viewed by ERS SAR. <http://www.ifm.uni-hamburg.de/ers-sar/>.

many of the interpretations of low backscatter regions associated with upwelling have been put forward without validating or supporting ancillary observations. *Apel* [1987] provided one of the earliest suggestions by associating relatively low backscatter regions imaged by SEASAT over the Nantucket Shoals off Cape Cod, Massachusetts, shown in Figure 9.2, with the presence of upwelling. In this case, upwelling is thought to be caused primarily by the interaction of the tidal and coastal currents with the shoals, which produces increased speed, turbulence, and significant mixing of the water column that lowers SST. Using ERS-1 data acquired off the island of Taiwan, *Hsu et al.* [1995] provided one of the first actual comparisons between SAR and sea surface temperature (SST) observations of upwelling activity. Figure 9.3 presents a two-frame ERS-1 SAR image acquired on 23 July 1994 and an AVHRR SST image acquired less than a day earlier over the East China Sea. The distinct low backscatter features correspond with low temperature features in the AVHRR data. These low temperature patterns routinely form off the coast of Taiwan and are interpreted as an indication of upwelling induced by Kuroshio Current interaction with the bathymetry [*Hsu et al.* 1995, 2000]. The presence of slicks, indicating biological activity, as well as of internal wave patterns, indicating the presence of stratification and a thermocline, is additionally captured by SAR. In spite of the evident detection potential of SAR, upwelling investigations using this technology have been very limited due in part to the difficulties in acquiring coincident thermal or ocean color observations that can be used to properly characterized the SAR detections over upwelling regions. The lack of sufficient validation data sets is due in part to a combination of physical factors such as the presence of non-optimum atmospheric conditions and significant SAR access and availability limitations as compared to other sensor data.

9.4 U.S. West Coast Upwelling

The U.S. west coast is one of the major upwelling regions in the world because of the presence of intense and persistent upwelling-favorable (northerly) winds. Significant upwelling research has been conducted in this region using thermal as well as ocean color spaceborne observations. In order to identify imagery that contained upwelling signatures, a search of RADARSAT-1 and ERS-1/2 SAR archived data available over the U.S. west coast for which image thumbnails were provided was done in the Canadian Centre for Remote Sensing (CCRS) Earth Observing Catalogue [CCRS, 2001] and the ESA Earth observation catalogue [ESA, 2001]. Although limited in spatial resolution and lacking optimal enhancement, the available thumbnails indicated the regular detection of many features consistent with upwelling activity in the region. Overall, the imagery found conveyed the potential that SAR has for coastal monitoring of the region.

Based on the thumbnail assessment, a full resolution RADARSAT-1 ScanSAR Wide image of the California coast south of Monterey Bay acquired on 3 May 1998 at 1410 UTC was obtained, a portion of which is shown in Figure 9.4. A region of lower backscatter and slick signatures along the coast can be seen, indicating upwelling activity. The upper and left side of the image shows a region dominated by high winds and atmospheric variability patterns. These atmospheric features increase the surface roughness and limit the SAR imaging of the low backscatter upwelling patterns.

AVHRR SST observations obtained during relatively clear conditions on 9 and 10 May show active upwelling from Monterey Bay to Point Conception, as indicated by the lower temperature waters (blue and greenish colors) along the coast seen in Figure 9.5. Additional SAR thumbnail images over the region show low backscatter SAR upwelling signatures along

Upwelling

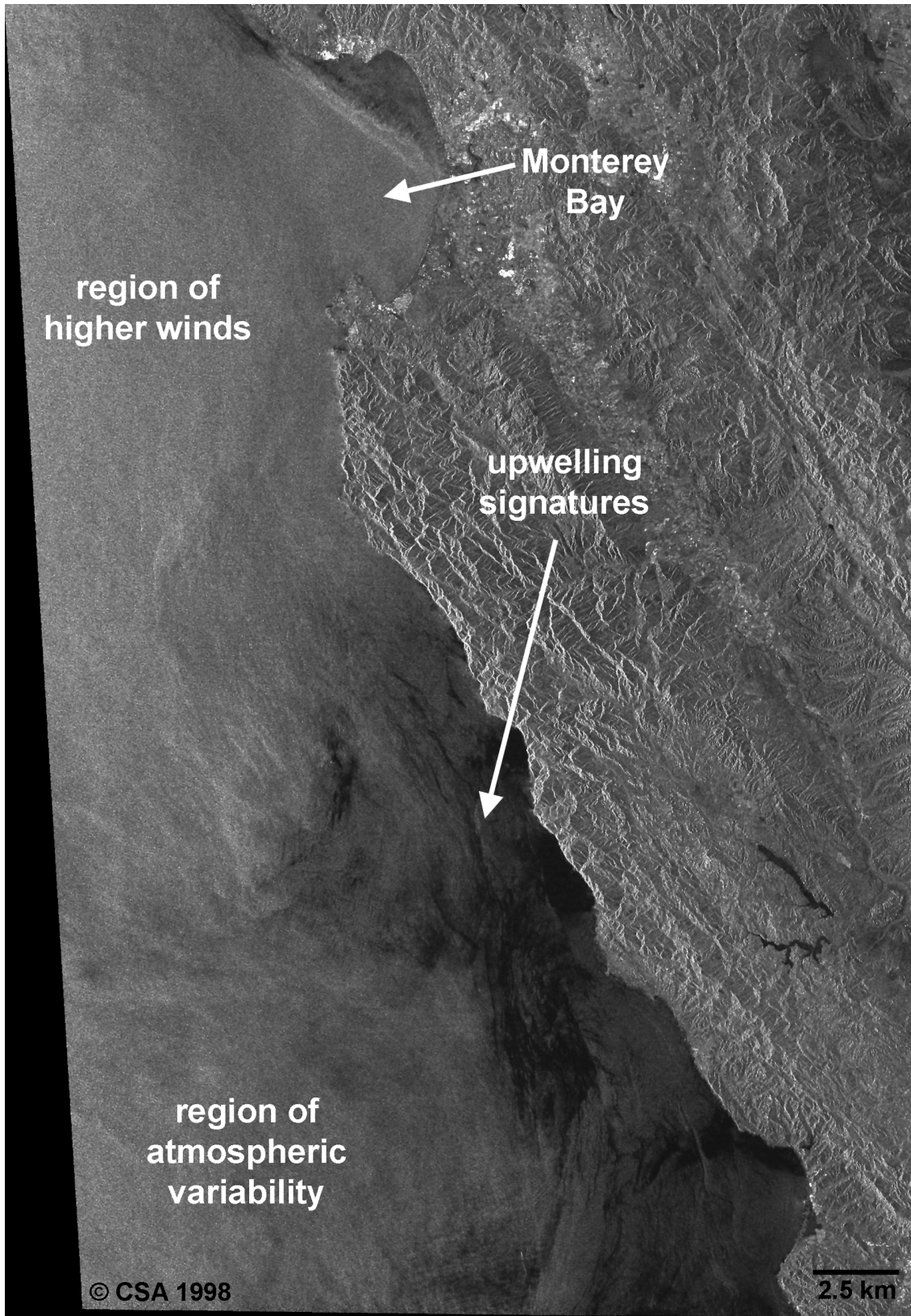


Figure 9.4. RADARSAT-1 (C-band, HH) ScanSAR Wide image of the California coast south of Monterey Bay on 3 May 1998 at 0157 UTC showing a low backscatter region and slick patterns associated with coastal upwelling.

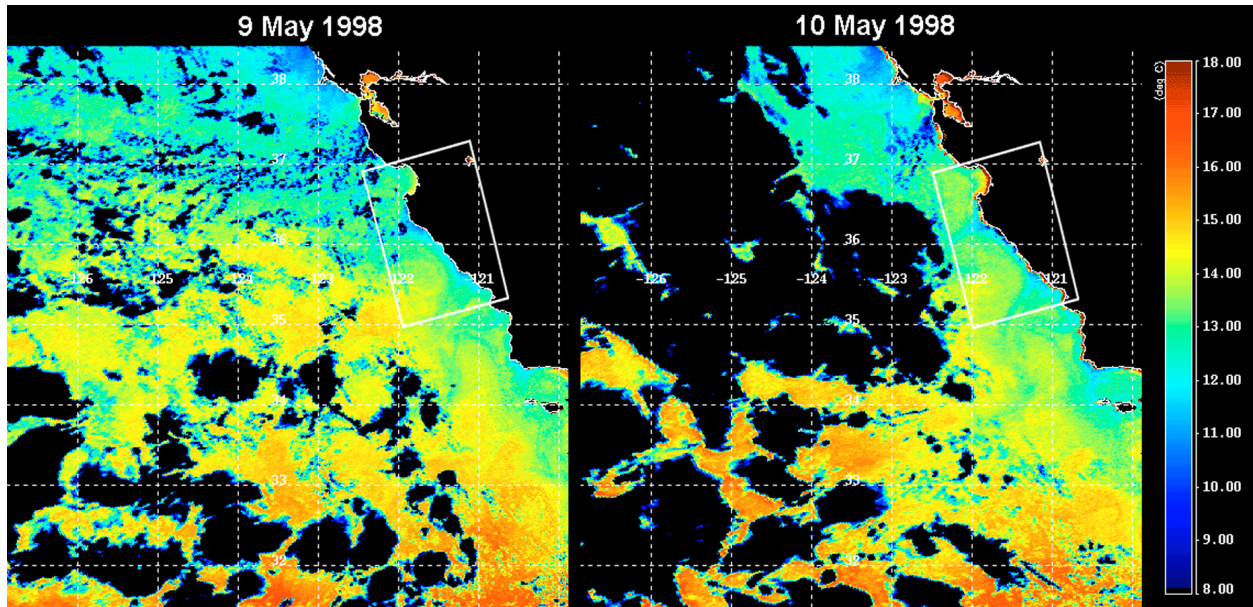


Figure 9.5. AVHRR images of SST off the California coast acquired on 9 May (left) and 10 May (right) 1998 at approximately 2100 UTC and showing upwelling activity south of Monterey Bay. The upwelling activity along the coast is indicated by the lower temperature waters (blue and greenish colors). *These images were obtained from the Monterey Bay Aquarium Research Institute Biological Ocean Group remote sensing data server, MBARI, 2001*

the coast, but are similarly limited in offshore extent. In fact, a preliminary assessment of the available SAR thumbnail imagery of the west coast suggests that observed SAR low backscatter patterns do not tend to delineate the full offshore extent of SST upwelling signatures in the region. That is, while SAR low backscatter patterns that correlate with upwelling thermal patterns were found near the coast, offshore thermal upwelling patterns do not appear to produce identifiable SAR signatures. The fact that the strongest SST coastal upwelling signals typically occur inshore and that strong winds (greater than approximately 10 m s^{-1}) tend to decrease ocean SAR signatures provides an explanation for the partial capture of upwelling features by SAR along the west coast. In other words, the same strong winds responsible for the extraordinary upwelling activity observed in this region may at the same time be hindering the imaging of the phenomenon by SAR.

Of course, atmospheric “contamination” of the SAR upwelling signature may not be limited to the offshore area but could also affect the observation of expected upwelling patterns inshore. This is shown in Figure 9.6 where convective cell signatures contaminate the upwelling lower backscatter and slick patterns. In spite of the potential complications from either low wind speed or other atmospheric or oceanic signatures, SAR has the potential to detect upwelling activity under certain conditions. However, to date there has been very limited upwelling research and applications development using this sensor. An early example of unpublished research was worked done by Pierre Flament as part of a NASA JPL project that looked at the detection of a coastal jet feature associated with West Coast upwelling conditions using airborne SAR and 1994 Shuttle SIR-C SAR data [Evans and Plaut, 1996]. A dissertation work on biological oceanography conducted by Paul DiGiacomo under the advice of Ben Holt appears to be one of the first to link SAR observed features with upwelling activity in the Southern California Bight (SCB) [DiGiacomo, 1999]. Figure 9.7 shows the ERS-1 SAR and AVHRR SST images of a small-scale cyclonic eddy observed in the Santa Monica Basin on 29 November

Upwelling

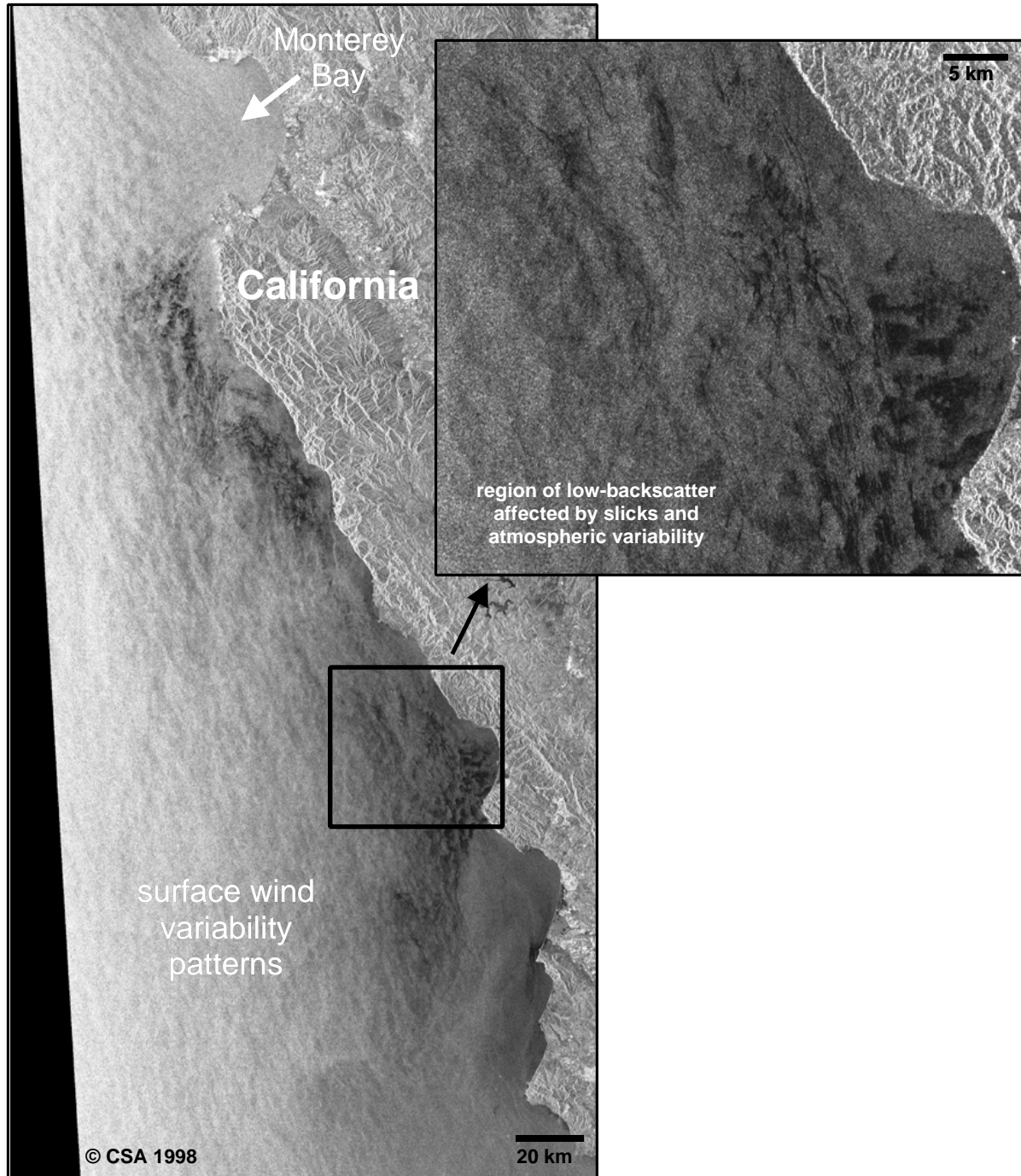


Figure 9.6. RADARSAT-1 ScanSAR Wide (C-Band, HH) image of the California coast south of Monterey Bay on 20 June 1998 at 0157 UTC showing low backscatter features associated with upwelling patterns contaminated by atmospheric conditions near the coast.

1994. The eddy, approximately 25 km in diameter, was interpreted by *DiGiacomo* to be associated with an upwelling event off Point Dume at the northwest edge of Santa Monica Basin. The cold eddy is delineated in the SAR image by counterclockwise spiraling slicks. Although in this case the slicks are interpreted as being of biogenic origin, the SCB is also characterized by

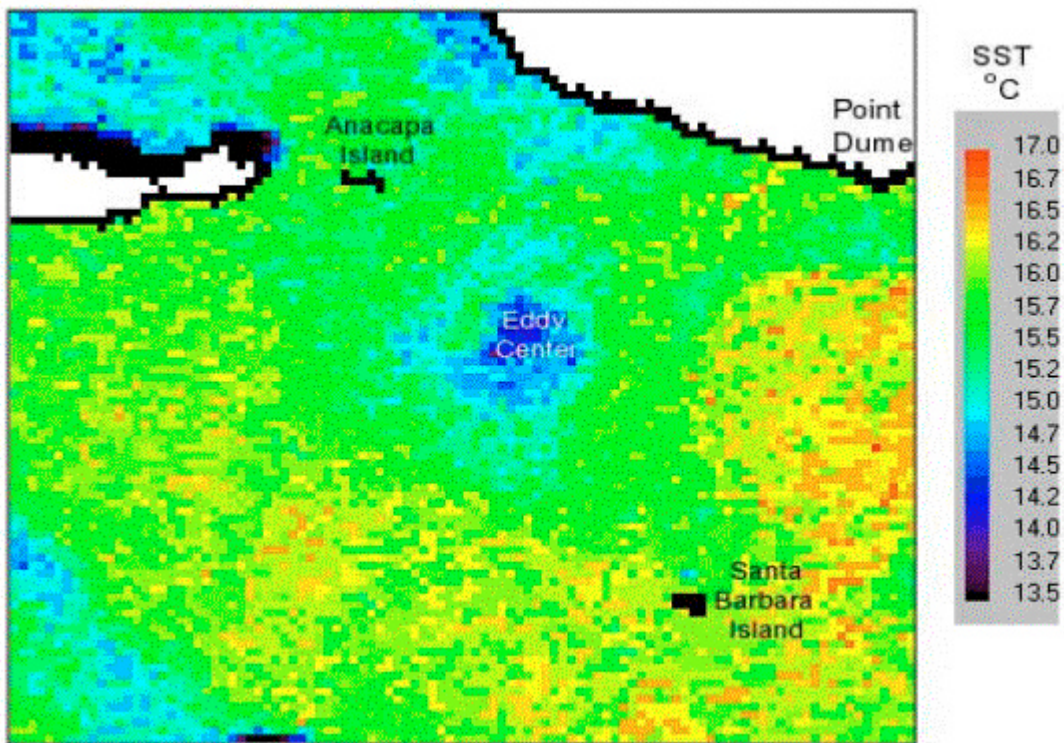
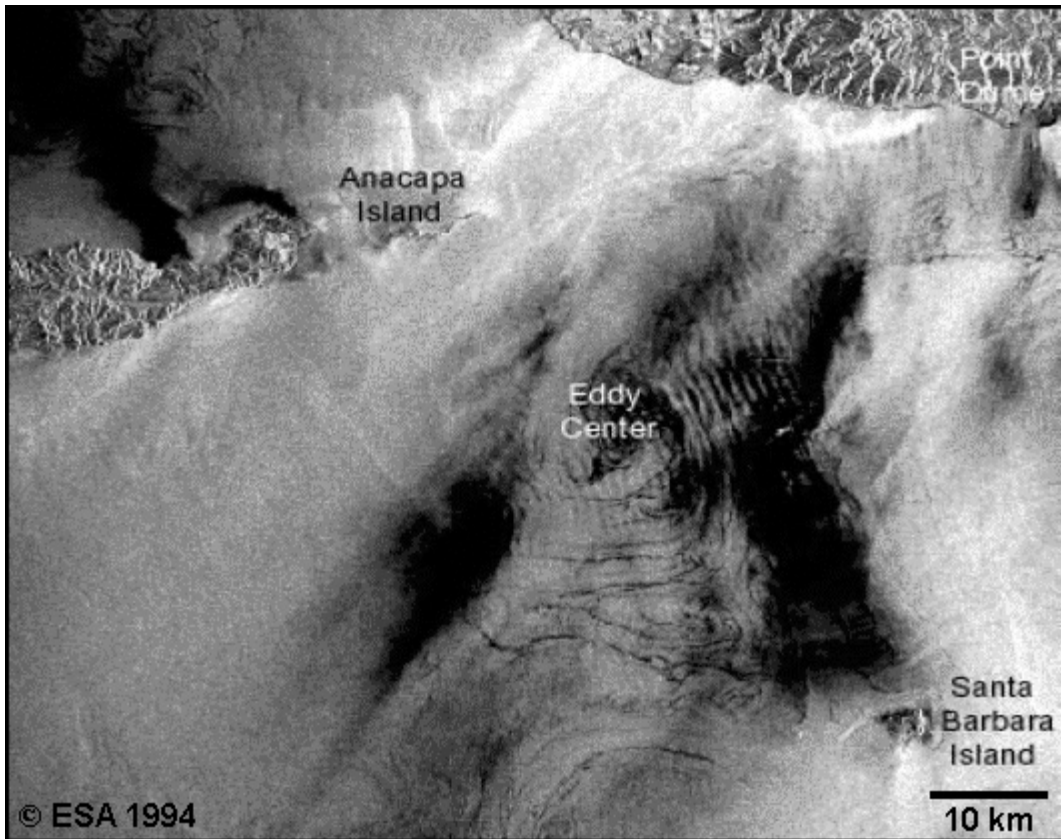


Figure 9.7. ERS-1 SAR image (above) of a cyclonic eddy in the Santa Monica Basin and near-coincident AVHRR SST image (below) of the same feature 2.5 hours earlier on 29 November 1994. The author associated the eddy with an upwelling event off Point Dume. [After DiGiacomo, 1999]

Upwelling

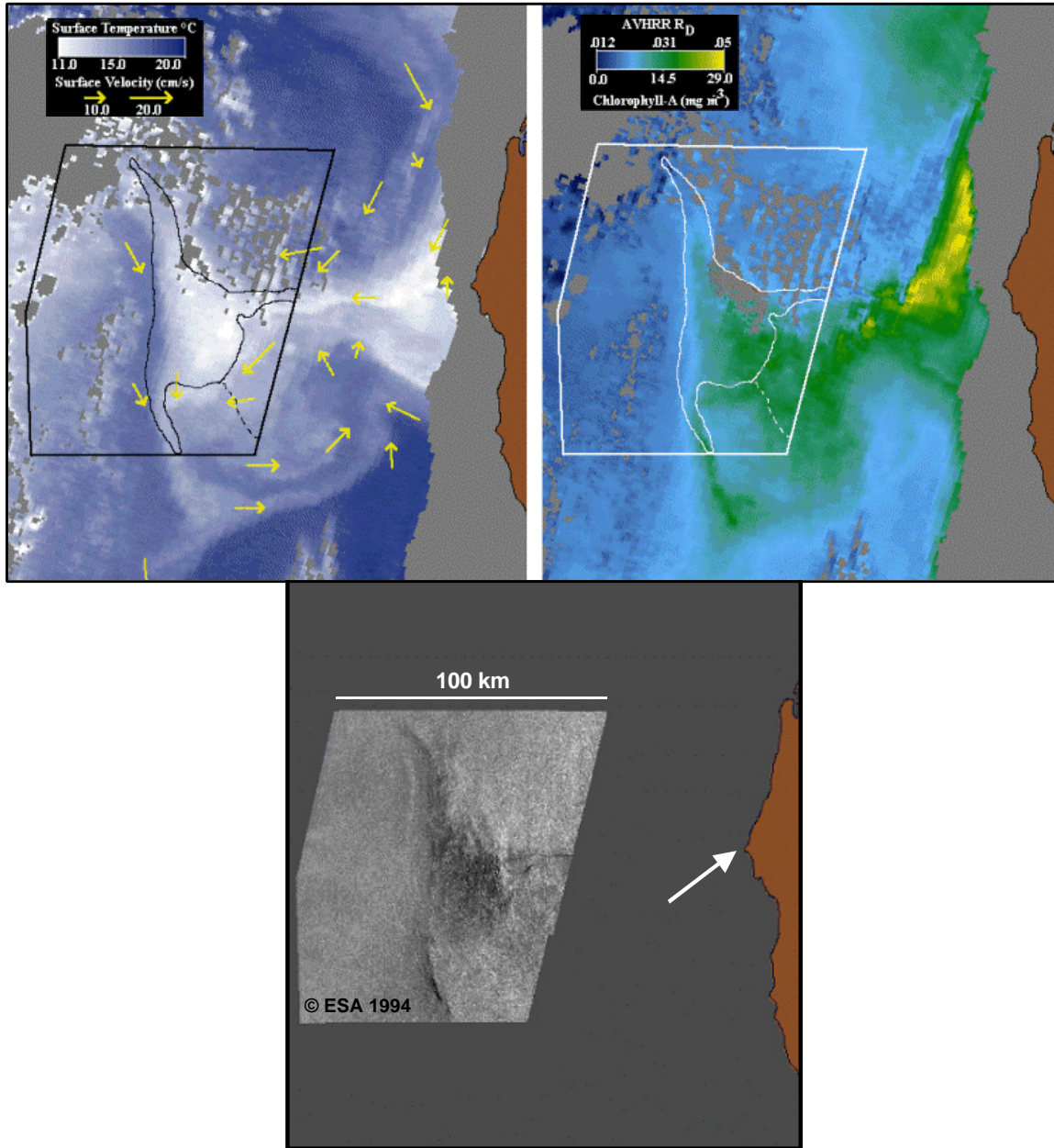


Figure 9.8. ERS-1 SAR and AVHRR images off Cape Blanco, Oregon, 26 August 1994; AVHRR SST (left), AVHRR chlorophyll estimate from the visible channel (right) and SAR (bottom). Circulation vectors were obtained from feature tracking on a series of AVHRR images. [After *Svejkovsky and Shandley, 2001*]

the widespread presence of natural mineral oil slicks that can also delineate circulation patterns. Thus, caution needs to be exercised in the interpretation of similar slick features in SAR imagery, as shown in Chapter 2 Figure 2.20 of this manual.

The Oregon State University GLOBEC Program in collaboration with Ocean Imaging has also looked at upwelling conditions to the north, off the Oregon-Washington coast. The program obtained 1994 ERS-1 and AVHRR images that captured upwelling-associated features. Based on these data, *Svejkovsky and Shandley* [2001] provided a comparison between coincident SAR observations. Figure 9.8 shows an upwelling filament as captured by ERS-1 SAR and AVHRR images acquired about 3 hours apart off Cape Blanco, Oregon, on 26 August 1994. In

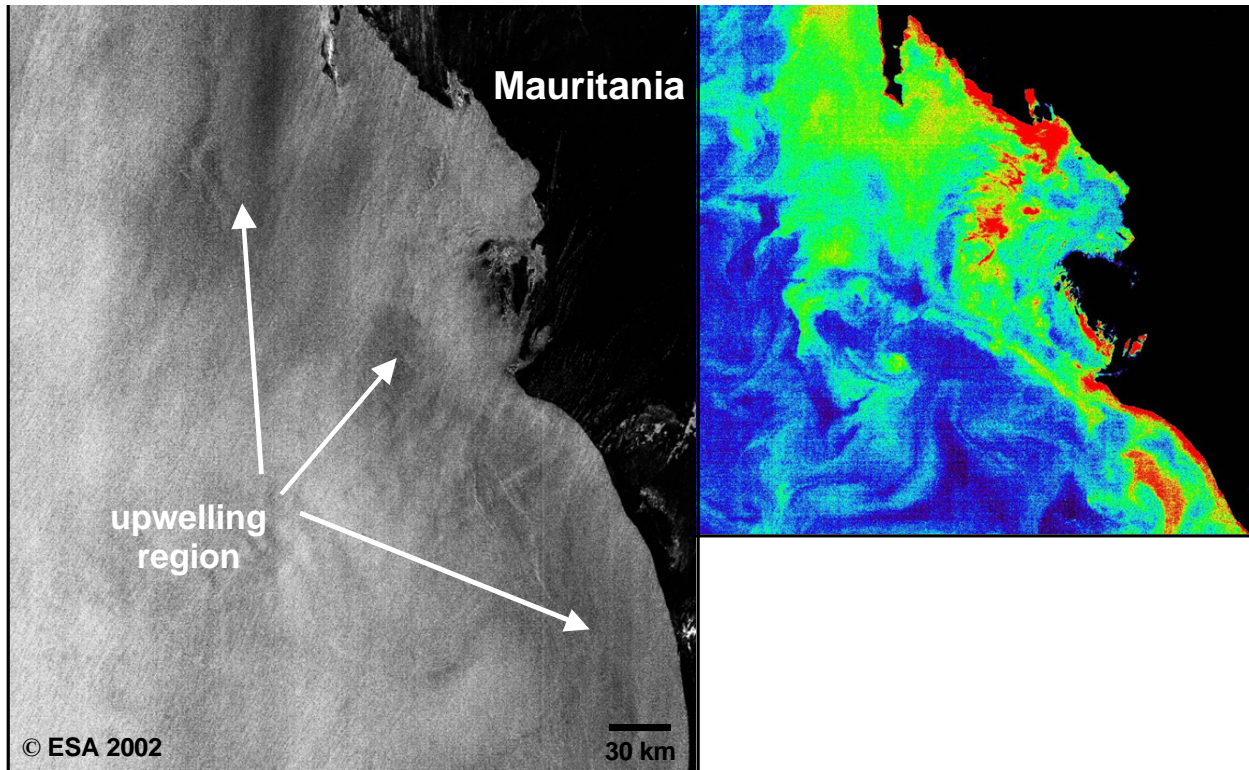


Figure 9.9. ENVISAT ASAR (C-band, VV) image (left) acquired off the coast of Mauritania in Northwestern Africa on 22 March 2002 along with a fluorescence product from MERIS ocean color data (right) simultaneously acquired. High biological activity associated with upwelling in the region is indicated by the red and green colors. [ENVISAT ASAR and MERIS images were acquired from the ESA's Observing the Earth web portal, ESA, 2002]

addition to the SST pattern, an AVHRR estimate of chlorophyll from the visible channel was produced that also matched the observed low backscatter area imaged by SAR, further pointing toward the biological nature of the upwelling filament.

Upwelling-favorable northerly wind forcing in the U.S. west coast is significantly stronger and more persistent than that experienced in the eastern coastal regions of the U.S. because of major atmospheric circulation patterns moving from the west over the Pacific Ocean. The offshore spatial extension of upwelling thermal (SST) or biological (ocean color) patterns is consequently much greater in the west coast than it would be in the east. In contrast, a closer match between the smaller SST and ocean color upwelling patterns observed off the east coast and their associated SAR low backscatter patterns has been found, as we will see in the next subsection.

Other strong upwelling areas characterized by strong winds should similarly exhibit apparent weakening of SAR upwelling detection offshore, as that observed off the west coast. An example of SAR observations of another major upwelling region is shown by the ENVISAT ASAR image of the coast of Mauritania in Figure 9.9. In this case, the presence of strong northerly winds at the time of the observation is indicated by the wind rows signatures in the image. Again, the presence of high winds, which produces excessive surface roughening and mixing, is responsible for the relatively weak contrast of the upwelling backscatter pattern than what would otherwise be expected over an active upwelling region. The occurrence of upwelling conditions in the region is confirmed in this case by the MERIS fluorescence data obtained simultaneously and also shown in the figure.

9.5 U.S. East Coast Upwelling

The U.S. east coast is one of many regions around the world that is impacted by localized seasonal upwelling events. Localized seasonal upwelling throughout the U.S. Middle-Atlantic Bight (MAB), from New England to the North Carolina Capes, occurs during the summer months (June to September) because of episodic wind forcing generally from the south. While upwelling events in the region are more confined and of less duration than over the west coast, they still are of local importance to the water mass distribution and productivity of the region. Because of the University of Delaware College of Marine Sciences interest in studying the interaction between coastal circulation and upwelling dynamics over the MAB continental shelf, a detailed investigation of upwelling detection by SAR was undertaken by NOAA/NESDIS that made available a large amount of full-resolution RADARSAT-1 SAR data over the U.S. east coast [*Clemente-Colón, 2001*]. Multiple RADARSAT-1 observations during periods of confirmed upwelling and non-upwelling conditions in June, July, and August 1998 have provided insight as to the ability of SAR to detect and monitor the phenomenon. Interpretation and validation of SAR upwelling observations were done using a series of available AVHRR SST, GOES IR, and SeaWiFS ocean color (Chl-a) images obtained before, during, or after the SAR observations. These data were supplemented by in-situ observations from weather buoys, Coastal-Marine Automated Network (C-MAN) stations and the Rutgers University Long-term Ecosystem Observatory off the coast of New Jersey.

Upwelling conditions off the Delaware Bay and the Chesapeake Bay were detected in three Standard Mode RADARSAT-1 SAR images on 2 June 1998 shown in Figure 9.10a. Near-coincident SST images indicate upwelling areas off the Delmarva (Delaware, Maryland, and Virginia) Peninsula down to the North Carolina coast, which developed in response to southerly winds. Low backscatter patterns imaged by SAR match closely the upwelling locations observed in the near-coincident SST data. Figure 9.10b shows a close-up of the southernmost upwelling feature in these SAR images revealing the substantial presence of slicks within the lower backscatter areas on the colder side of the isotherms. Donato and Marmorino [2002] provide further analysis of this coastal feature. Through a semi-analytical approach, the sensitivity of the radar backscatter to SST over “slick-free” waters has been found to be of the order of $1^{\circ}\text{C}/\text{dB}$ and is attributed mostly to changes in the marine boundary layer stability, i.e., a decrease in the turbulent flow and consequently in the wind stress over cooler waters. It was also noted that this radar sensitivity to SST changes decreases as wind speed increases [*Clemente-Colón, 2001*]. When slicks are present, extremely low backscatter values are observed, in some cases down to the noise floor of the instrument. The upwelling-associated biogenic surfactants are in fact very effective in damping Bragg waves and in many cases dominate the SAR imaging of upwelling patterns.

An apparent detachment or coastal separation of the location of upwelling low backscatter features off the Chesapeake Bay and Delaware Bay mouths is also noted and can be observed in more detail in Figures 9.10c and 9.10d. The edge of the SAR upwelling patterns sharply delineates the offshore frontal extent of a bay outflow and southward coastal flow feature in both cases. It can be expected that the presence of upwelling activity in the vicinity of an estuary outflow would impose restrictions or boundary conditions on the development and surface manifestation of each other. The impact of both, atmosphere-ocean interactions and the buoyant low salinity outflows, on the circulation dynamics of this region are further addressed by *Austin and Lentz, [1999]* and *Rennine et al., [1999]*.

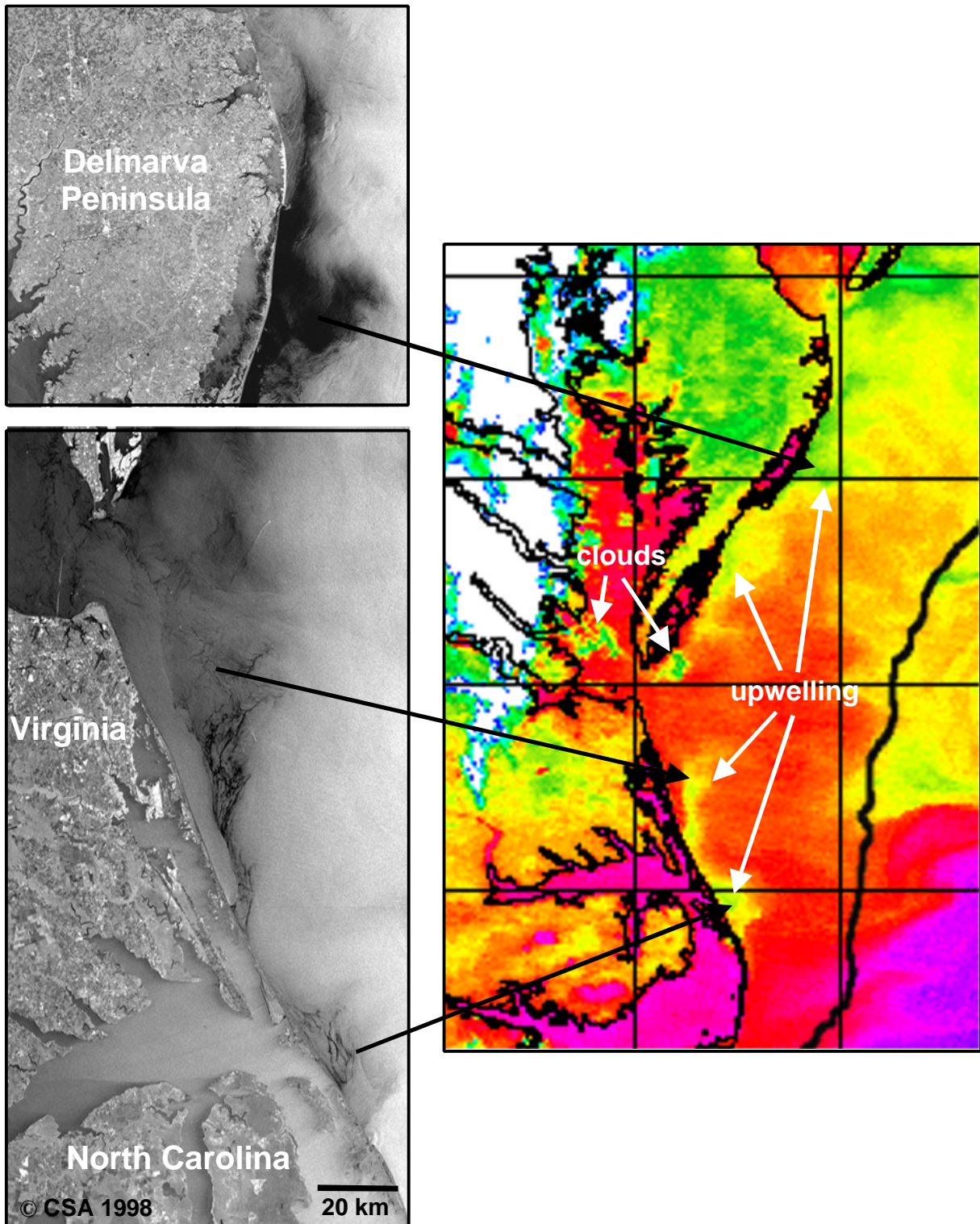


Figure 9.10a. Coastal upwelling activity from the Delaware Bay to the North Carolina coast as imaged by RADARSAT-1 Standard Mode (C-Band, HH) frames at about 1115 UTC (left) and AVHRR SST ($^{\circ}\text{C}$) at 1108 UTC (right) on 2 June 1998. The dark line offshore in the AVHRR image represents the 100m isobath and indicates the extent of the continental shelf.

Upwelling

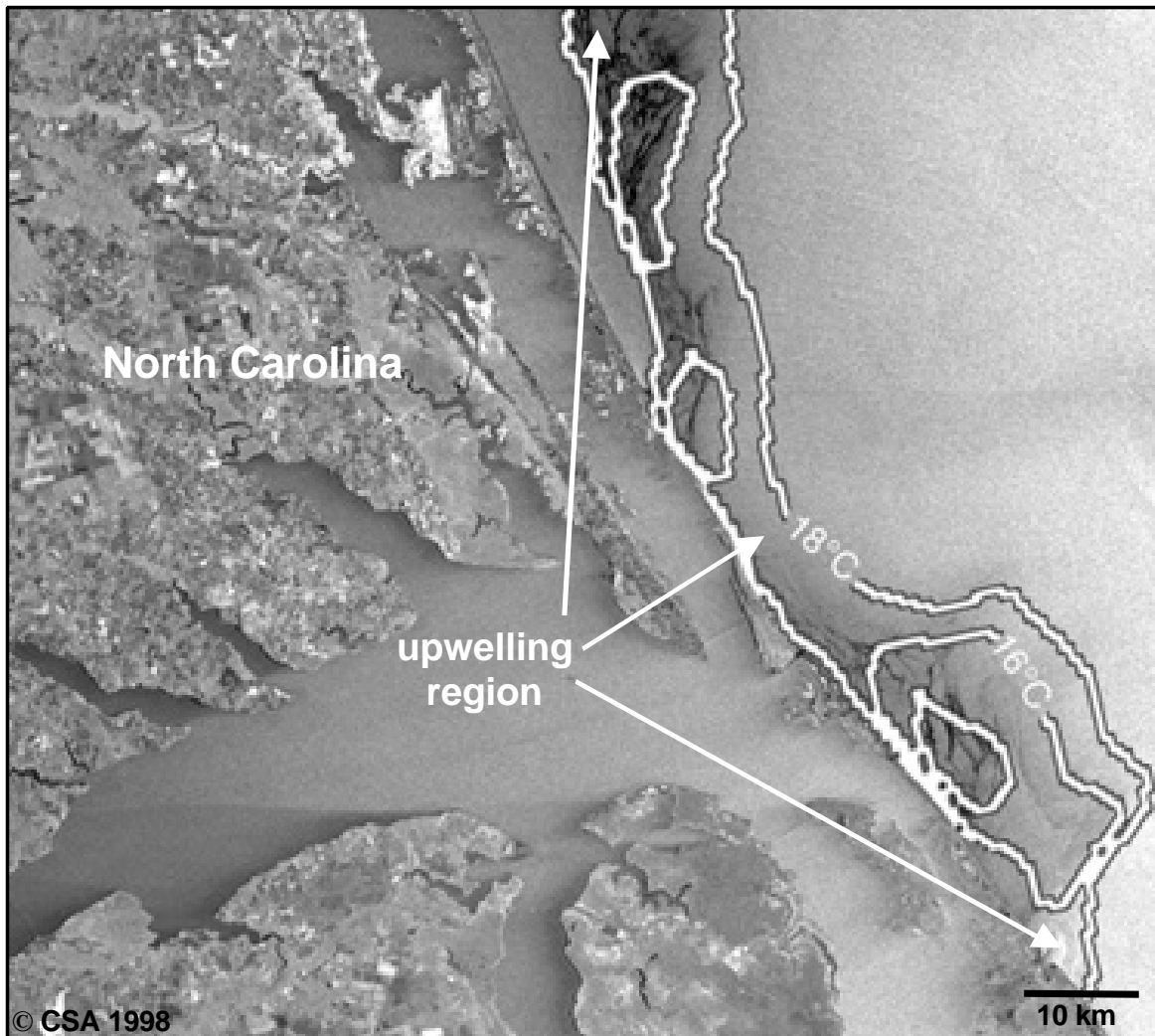


Figure 9.10b. Close-up of upwelling activity off the North Carolina coast as imaged by SAR on 2 June 1998 at 1115 UTC with the 18°C and 16°C isotherms from AVHRR data acquired at 1108 UTC superimposed.

Upwelling along the coasts of New Jersey and Long Island was relatively intense on 30 July 1998 due to persistent winds and was captured by both RADARSAT-1 SAR and AVHRR SST as shown in Figure 9.11a. The data show a direct correspondence between the low backscatter SAR and low SST patterns along the upper coast of New Jersey and the southern coast of Long Island. In addition, the SAR image shows a large filament pattern that extends southward from the Long Island coast as well as noticeable large low backscatter patterns in the middle of the image over the outer continental shelf. The outer low backscatter regions correspond closely with SeaWiFS Chl-a concentration observations (Figure 9.11c) rather than with SST.

Figure 9.11b shows a close-up of the SAR observations off the upper New Jersey coast and the Hudson River Estuary revealing the location of several distinct upwelling centers, slick patterns associated with the upwelling filament extending off Long Island as well as a Hudson River Estuary plume front. Similar to the observations off the Delmarva Peninsula (Figure 9.10c), the low backscatter areas along the New Jersey coast correspond to lower SST temperatures. Again, the lower backscatter is caused by the cooler upwelled waters and the

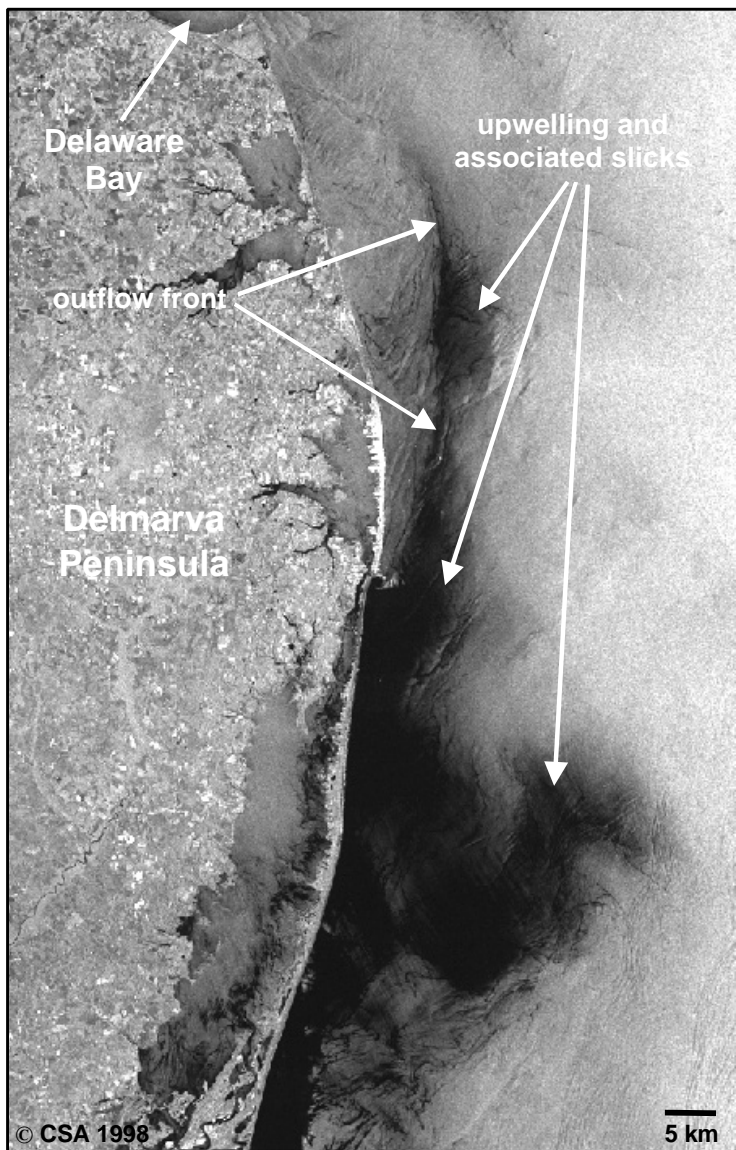


Figure 9.10c. Close-up of upwelling activity off the Delaware Bay mouth as imaged by SAR on 2 June 1998 at 1115 UTC.

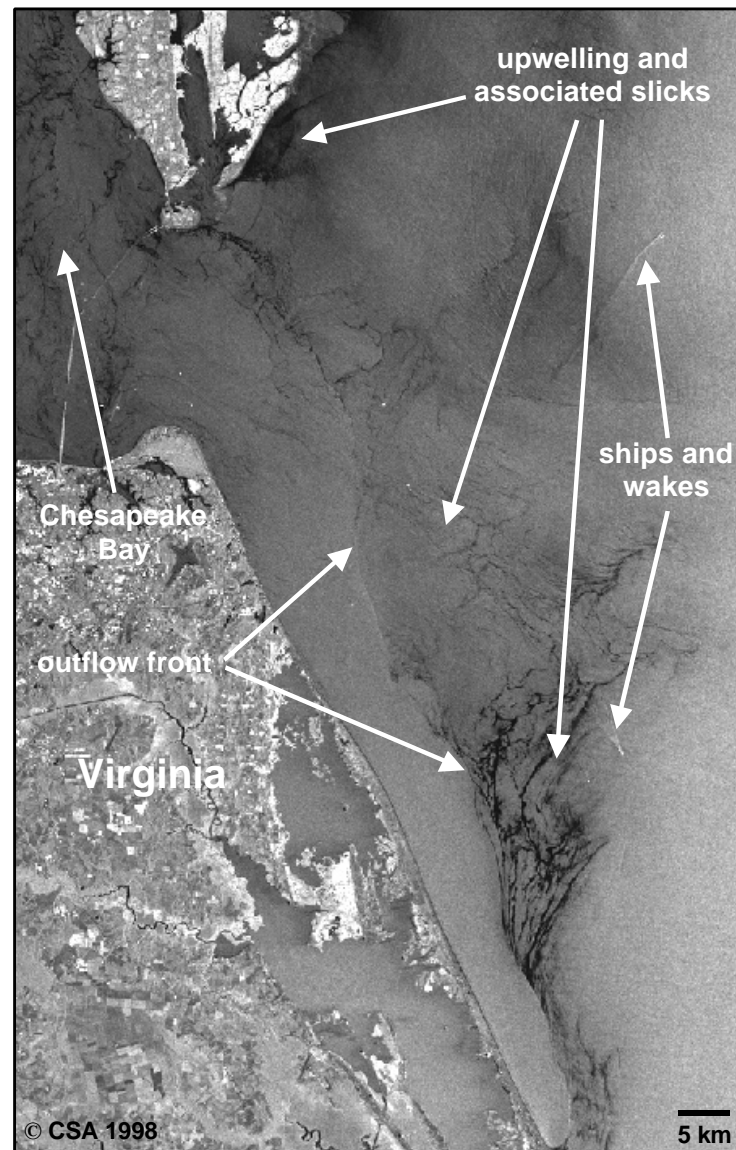


Figure 9.10d. Close-up of upwelling activity off the Chesapeake Bay mouth as imaged by SAR on 2 June 1998 at 1115 UTC.

Upwelling

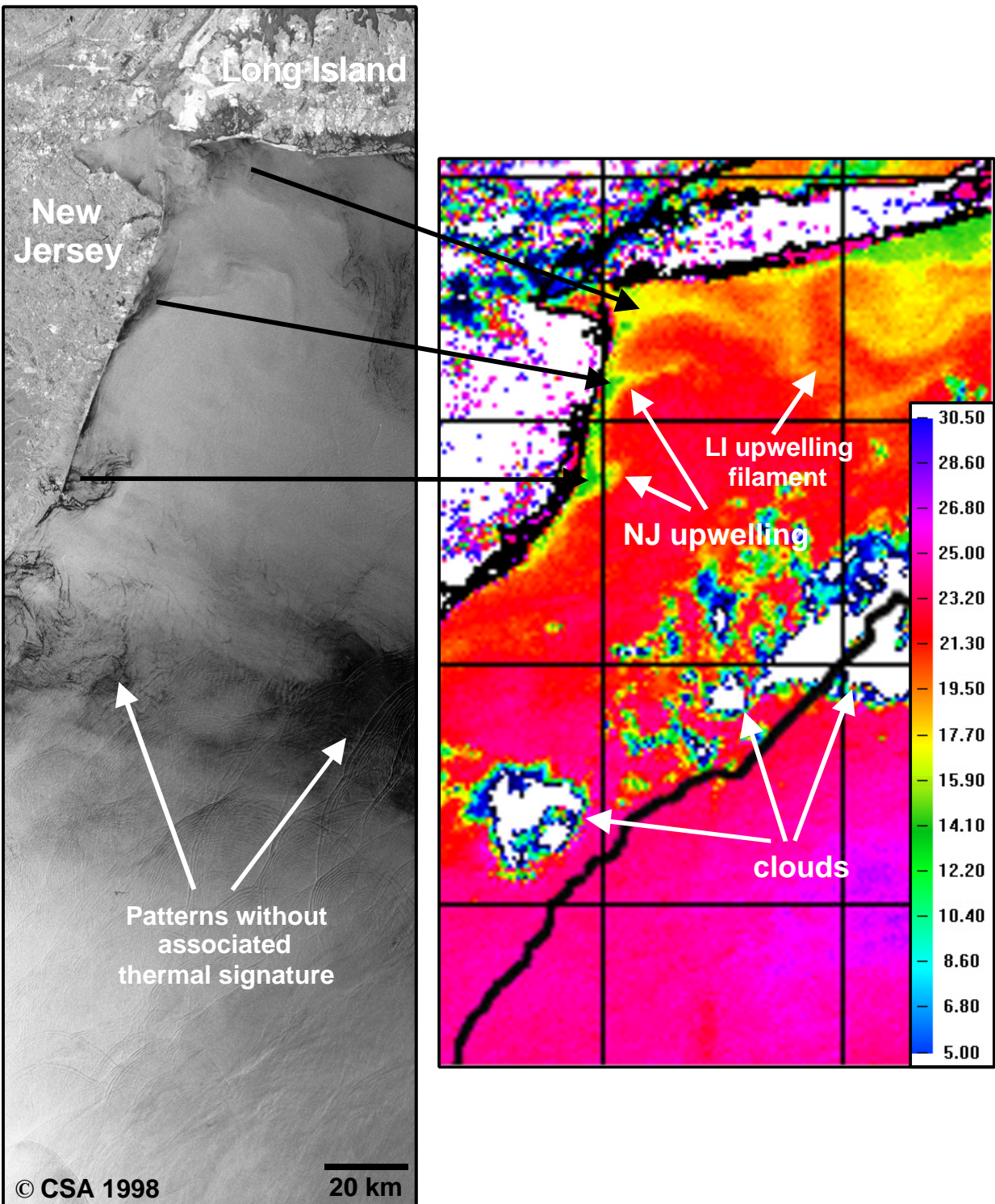


Figure 9.11a. Upwelling activity off the upper New Jersey and Long Island coasts as imaged by RADARSAT-1 (C-band, HH) Standard Mode at 2240 UTC (left) and AVHRR SST (in °C) at 1832 UTC (right) on 30 July 1998. The dark line offshore in the AVHRR image represents the 100m isobath and indicates the extent of the shelf.

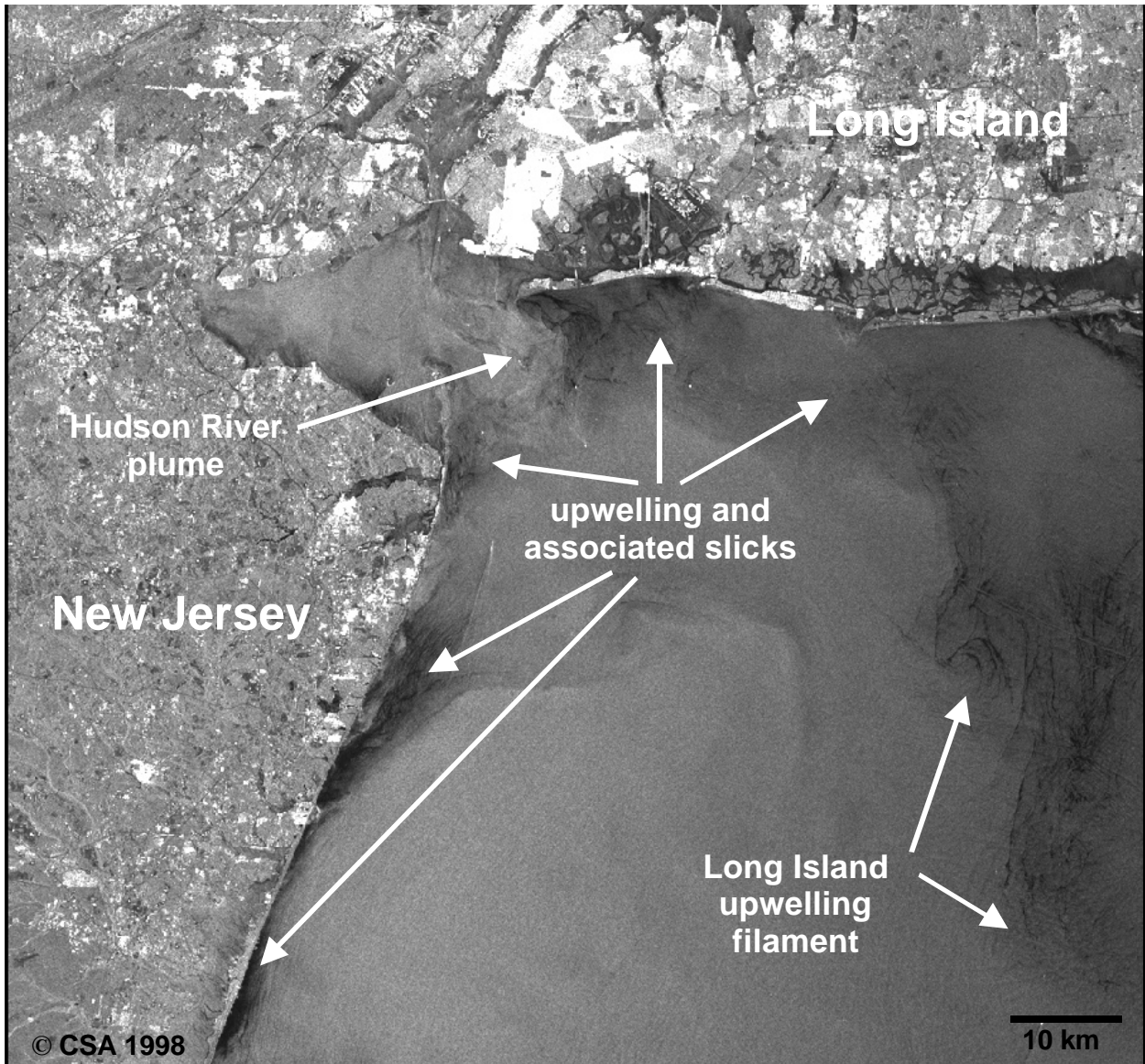


Figure 9.11b. Close-up of upwelling activity and offshore filament patterns off the New Jersey coast, the Hudson River Estuary, and the southern coast of Long Island as imaged by RADARSAT-1 (C-band, HH) Standard Mode on 30 July 1998 at 2240 UTC.

presence of biogenic surfactants. The image also shows a sharp frontal region between the warmer and fresher estuarine waters of the Hudson River and the colder and saltier shelf waters similar to the patterns off the Delaware and Chesapeake Bays in Figure 9.10c and 9.10d. In the SAR image, the Long Island cold filament is characterized by the delineation of eddy circulation patterns by surfactants as it extends southward. The filament is also observed in the SeaWiFS Chl-a concentration data extending southward past mid-shelf (Figure 9.11c) along with two other offshore bloom features that correspond closely with the offshore low backscatter patterns visible in SAR image (Figure 9.11d). This close correlation supports the interpretation of both of these SAR features as being in fact manifestations of offshore biological activity resulting as a secondary effect of the coastal upwelling activity. Internal waves imaged in the blooms, indicating the presence of stratification conditions below, are also noteworthy.

Upwelling

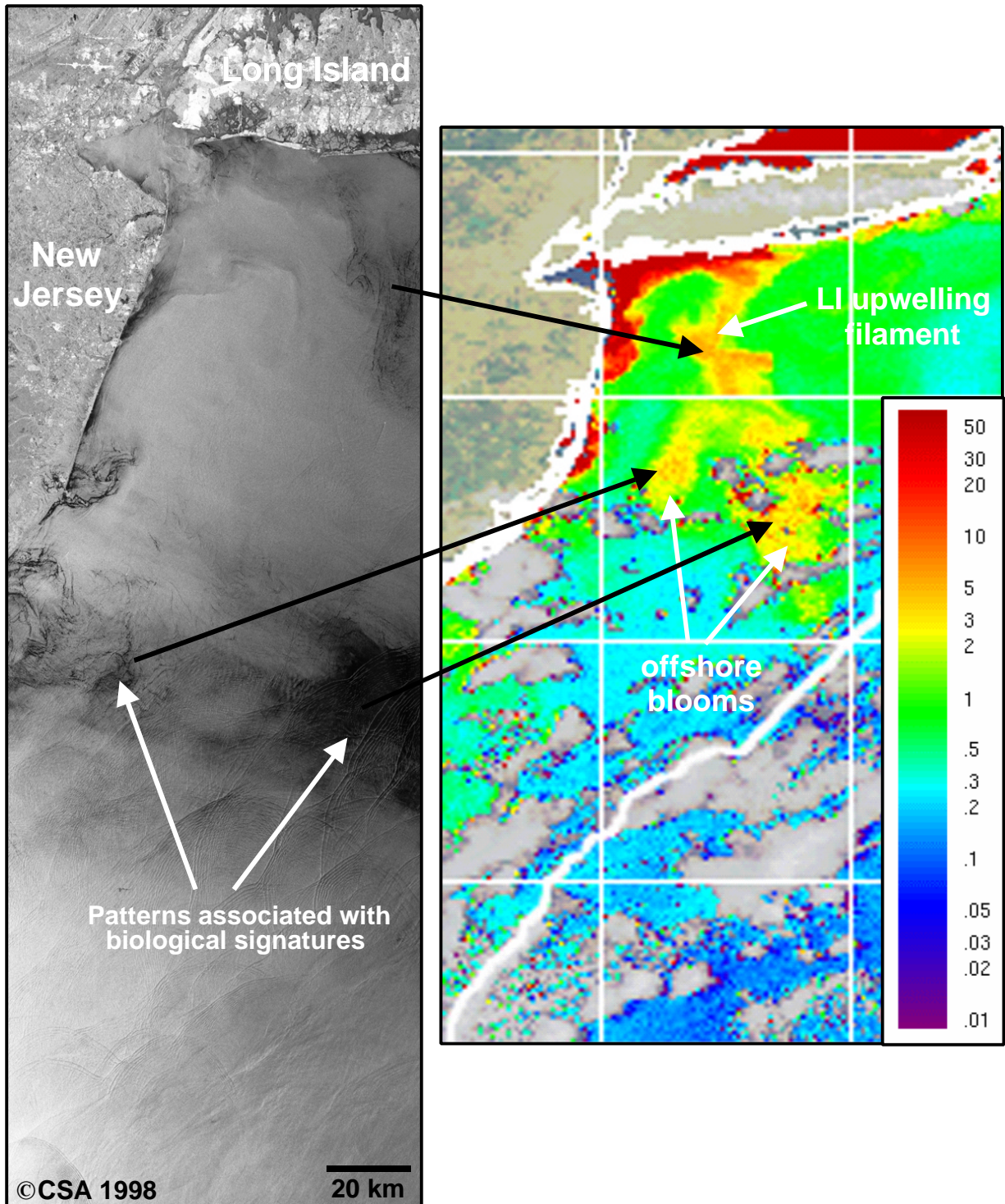


Figure 9.11c. Upwelling and offshore bloom patterns in a SeaWiFS Chl-a (in mg m^{-3}) image (right) of upper New Jersey, the Hudson River Estuary, and Long Island from 2 August 1998 at 1713 UTC compared against the 30 July RADARSAT-1 SAR (C-Band, HH) observations (left). The white line offshore in the SeaWiFS image represents the 100m isobath and indicates the extent of the shelf.

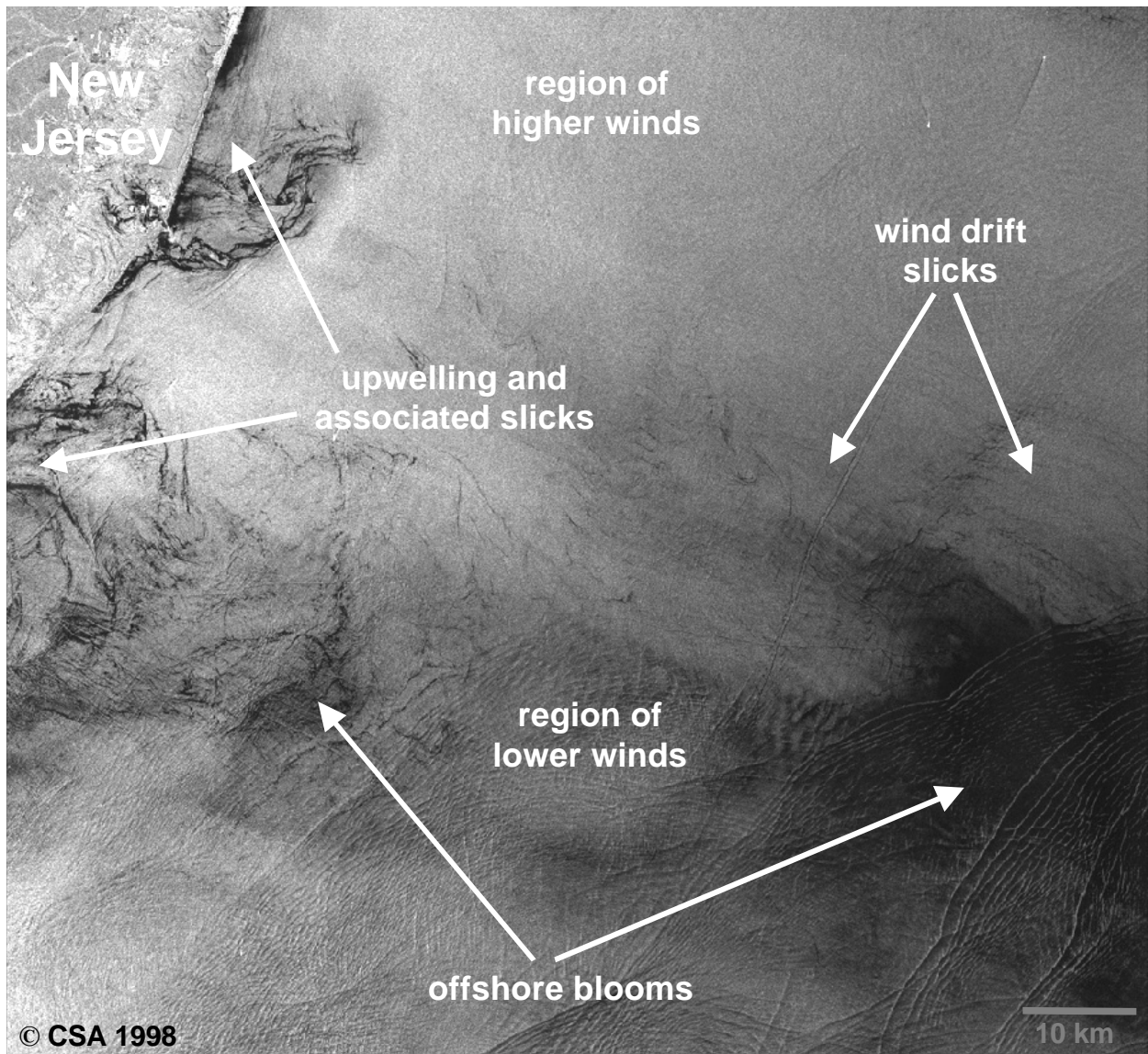


Figure 9.11d. Close-up of upwelling and offshore bloom features off the New Jersey coast imaged by RADARSAT-1 (C-band, HH) Standard Mode on 30 July 1998 at 2240 UTC.

A series of observations over the Nantucket Shoals upwelling region off Cape Cod were also available as part of the 1998 MAB data studied. Both SST and ocean color imagery captured a recurrent upwelling center sustained mainly by the coastal current interaction with the shoaling bathymetry. An example of SAR's ability to closely delineate this upwelling feature is shown by the near-coincident RADARSAT-1 and NOAA AVHRR SST observations off Cape Cod on 13 August 1998 in Figure 9.12a. A well-defined upwelling region observed in the sea surface thermal data is in strong agreement with the observed low backscatter pattern shown also in a close-up in Figure 9.12b. These data support *Apel's* [1987] interpretation of an upwelling induced decrease in backscatter in the 1978 SEASAT data (Figure 9.2). In addition to the low backscatter conditions imposed by the presence of upwelling, multiple bright bathymetry signatures generated over the Nantucket Shoals are imaged. These features are the result and confirm the presence of a shallow bathymetry and a strong flow over the region. The presence of

Upwelling

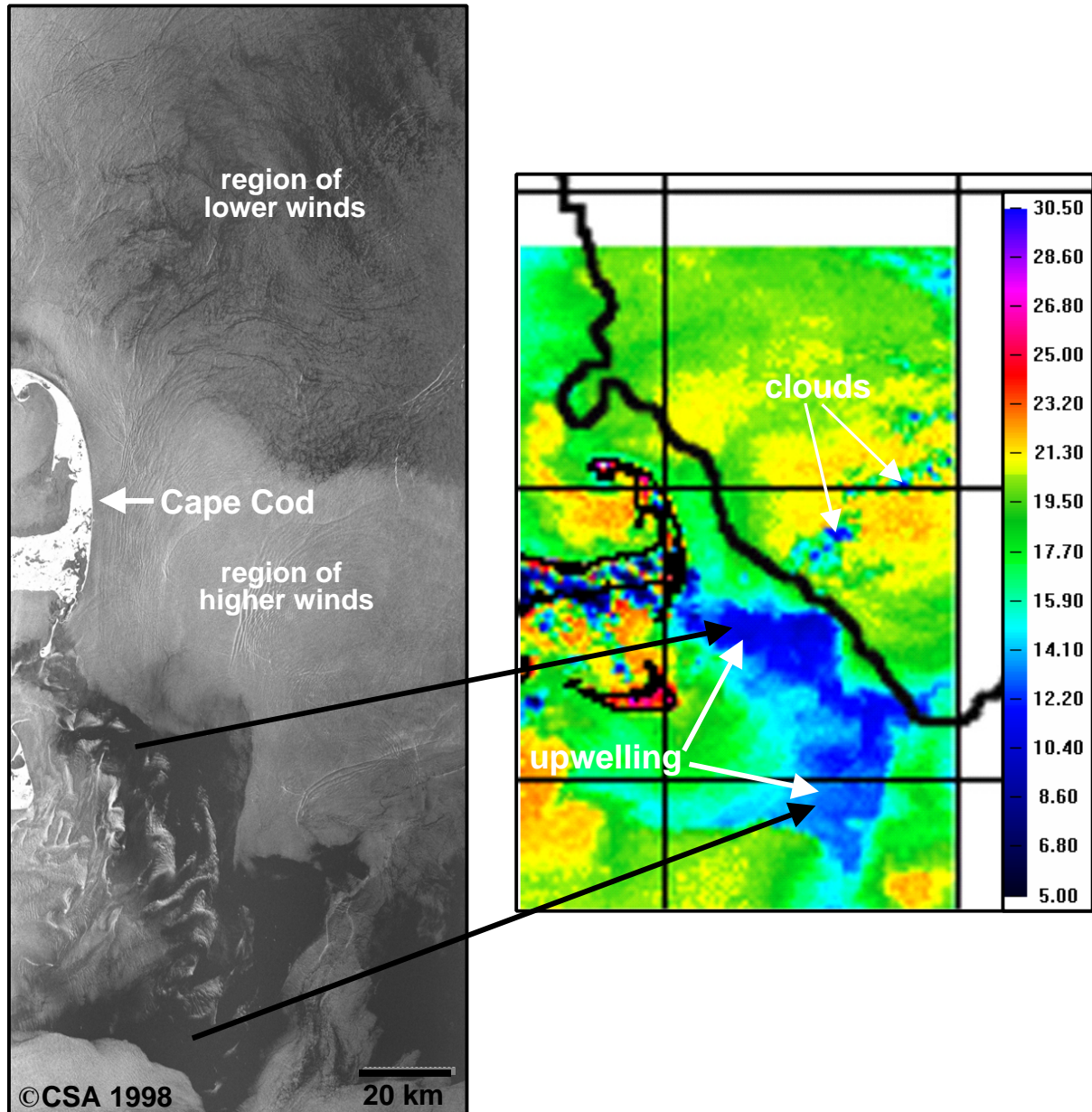


Figure 9.12a. Upwelling activity over the Nantucket Shoals as imaged by RADARSAT-1 (C-Band, HH) Standard Mode at 2232 UTC (left) and AVHRR SST (in °C) at 1906 UTC (right) on 13 August 1998. The dark line offshore in the AVHRR image represents the 100m isobath and indicates the extent of the shelf.

oceanic internal wave packets to the north indicates stratified conditions in the area. In addition, lower wind speeds over the upper region in the image allows for the SAR imaging of biogenic slicks that are not directly associated with the upwelling conditions.

9.6 Summary

The coincident and near-coincident SAR, SST, and ocean color observations shown in this chapter demonstrate the ability of SAR to detect upwelling patterns in major (e.g. U.S. west coast) and minor (e.g. U.S. east coast) regimes. The potential for offshore imaging in major

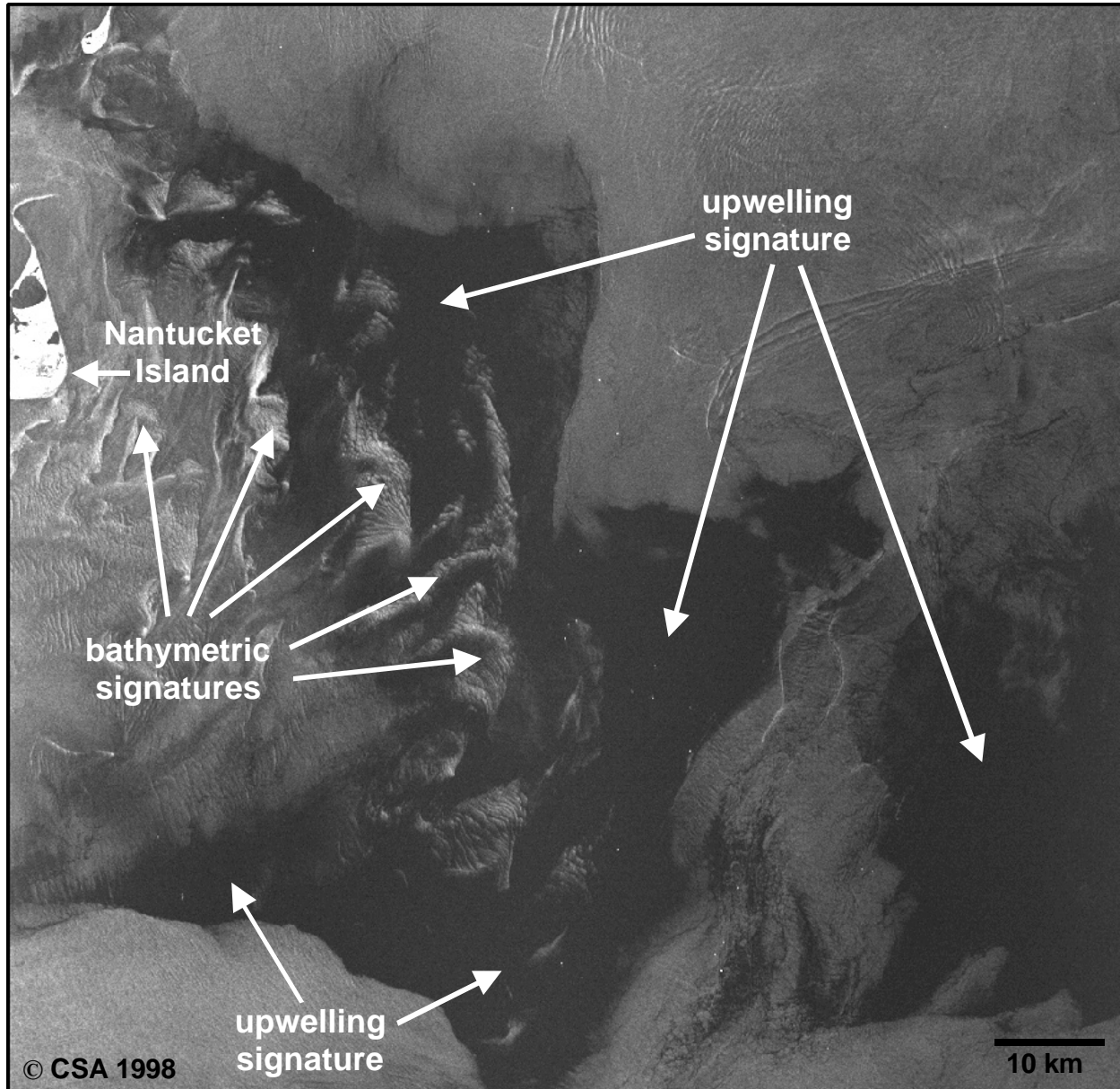


Figure 9.12b. Close-up of Cape Cod upwelling pattern as imaged by RADARSAT-1 (C-band, HH) Standard Mode on 13 August 1998 at 2232 UTC.

upwelling regions may be diminished by the prevalence of associated stronger or more prevalent winds. In fact, SAR appears to provide better imaging of upwelling patterns over minor wind-forced as well as current-induced upwelling areas than over major upwelling regions. In general, the presence of colder waters resulting from upwelling coincides with an overall decrease in backscatter due to an increase in the boundary layer stability that in turn produces a decrease on the wind stress. The presence of slicks associated with enhanced biological activity in upwelling regions significantly contributes to an additional decrease in the observed radar return through the effective damping of the Bragg waves. In addition, SAR can delineate circulation patterns associated with upwelling and other coastal processes through current modulation as well as the imaging of slick patterns.

Upwelling

When wind speed conditions are optimum SAR for observation, the fine spatial resolution of the sensor, compared to present spaceborne SST ocean color data, may provide better delineation of upwelling fronts. The ability of SAR to detect other ocean features such as internal waves, coastal fronts, and plumes, provides additional information that can be useful in the analysis of the upwelling region, particularly as it relates to the interaction between upwelling and these dynamical processes. Because of its ability to provide observations through clouds, SAR can help increase the available monitoring capabilities already provided by both IR and visible satellite sensors. Thus, SAR observations could help decrease temporal gaps in the monitoring of coastal upwelling conditions while providing a connection between thermal and biological observations as well as between upwelling and other coastal processes at different spatial scales.

However, it is clear that SAR observations of upwelling conditions are best interpreted when additional ancillary data such as SST or ocean color data are available. When combining SAR with these ancillary observations to interpret the presence of upwelling activity, it is important to keep in mind a number of caveats. First, thermal and ocean color upwelling observations do not always correlate with each other, i.e., although their dynamics may be linked initially, the evolution of SST and Chl-a may ultimately not. Thus, pattern mismatches between SAR and SST and between SAR and Chl-a observations should be expected. Second, although an abundance of natural slicks is characteristic of regions of enhanced biological activity, observations of increased Chl-a may not in fact directly correlate with the presence of slicks in SAR since the appearance of slicks may also depend on the degree of development of the biological activity as well as the wind conditions at the time of the observation. Third, ocean color observations indicating various degrees of biological activity are possible throughout the year, particularly in the coastal ocean, and may not indicate by themselves a response to enhanced upwelling activity in a region. And fourth, given that the presence of surfactants in seawater is indeed prevalent, including both biogenic and mineral substances, very low wind speed conditions can allow for the appearance of natural slicks to occur even when no upwelling-enhanced biological activity is present.

In summary, the capability of SAR should be used to complement the classical and widely accepted ways of monitoring upwelling phenomena such as in-situ observations of wind and ocean parameters or satellite observations of SST and ocean color. The addition of SAR as an upwelling observing tool should help improve our understanding of upwelling associated physical and biological coastal processes. These processes may include the distribution of biological productivity, the effect of enhanced productivity on the development of hypoxic conditions, water clarity, water mass exchange across the shelf, coastal outflow and currents, larval distribution and dispersion, and the dispersion and detection of pollutants, among others.

9.7 References

- Apel, J. R., 1987: *Principles of Ocean Physics*, Academic Press, Ltd., London, 634 pp.
- Austin, J.A., and S.J. Lentz, 1999: The relationship between synoptic weather systems and meteorological forcing on the North Carolina inner shelf, *J. Geophys. Res.*, **104(C8)**, 18,159-18,185.
- CCRS, 2001: Canadian Centre for Remote Sensing Quicklook Swath Browser. [<http://quicklook.ccrs.nrcan.gc.ca>]

- Clemente-Colón, P., 2001: Coastal Oceanography Applications of Spaceborne Synthetic Aperture Radar (SAR) in the Middle Atlantic Bight (MAB), *A Dissertation for the degree of Philosophy Doctorate*, College of Marine Studies, University of Delaware, Newark, Fall 2001, 233 pp.
- , and X.-H. Yan, 2000: Low backscatter features in SAR imagery, *JHU/APL Tech. Digest*, January-March, **21(1)**, 116-121.
- DiGiacomo, P.M., 1999: *Satellite Observation of Phytoplankton Variability in the California Current System: El Niño to Eddies*, Ph.D. dissertation, University of California, Los Angeles.
- Donato, T.F., and G.O. Marmorino, 2002: The surface morphology of a coastal gravity current, *Cont. Shelf Res.*, **22(1)**, 141-146.
- Ekman, V.W., 1905: On the influence of Earth's rotation on ocean current, *Ark. Mat. Astr. Fys.*, **2(11)**, 1-52.
- ESA, 2001: ESA Open Distributed Information & Services for Earth Observation (ODISSEO). [<http://odisseo.esrin.esa.it/>]
- , 2002: ESA Observing the Earth. [<http://www.esa.int/export/esaSA/earth.html>]
- Evans, D.L. and J.P. Plaut (eds.) 1996: Science Results from the Spaceborne Imaging Radar-C/X-Band Synthetic Aperture Radar (SIR-C/X-SAR): Progress Report, Jet Propulsion Laboratory, Pasadena, California. [<http://southport.jpl.nasa.gov/ProgressReports0496>]
- Fu, L.-L. and B. Holt, 1982: *Seasat Views Ocean and Sea Ice with Synthetic Aperture Radar*, NASA/JPL Publication 81-120, Feb. 15, 200pp.
- Hsu, M.-K., L.M. Mitnik, and C.-T. Liu, 1995: Upwelling area northeast of Taiwan on ERS-1 SAR images, *Acta Ocenogr. Taiwanica*, **34(3)**, 27-38.
- , A.K. Liu, and C. Liu, 2000: A study of internal waves in the China Seas and Yellow Sea using SAR, *Continental Shelf Res.* **20** (4-5), 389-410.
- MBARI, 2001: Monterey Bay Aquarium Research Institute Biological Ocean Group remote sensing data server. [http://www.mbari.org/bog/Projects/Satellite/seawifs_br/]
- Rennine, S.E., J.L. Largier, and S.J. Lentz, 1999: Observations of a pulsed buoyancy current downstream of Chesapeake Bay, *J. Geophys. Res.*, **104(C8)**, 18,227-18,240.
- Smith, R.L., 1968: Upwelling, *Oceanogr. Mar. Biol. Ann. Rev.*, **6**, 11-46.
- Svejkovsky, J. and J. Shandley, 2001: Detection of offshore plankton blooms with AVHRR and SAR imagery, *Int. J. Rem. Sens.*, **22**, 471-485.
- Yoshida, K., and H.-L. Mao, 1957: A theory of upwelling of large horizontal extent, *J. Mar. Res.*, 16, pp. 40-54. Republished in *Selected Scientific Papers of Professor Kozo Yoshida*, Lab. of Phys. Oceanogr., Geophys. Inst., U. of Tokyo, 1978, 134-148.